doi:10.1093/brain/awy044 BRAIN 2018: 141; 1470–1485 | 1470

BRAIN
A JOURNAL OF NEUROLOGY

Electromagnetic signatures of the preclinical and prodromal stages of Alzheimer's disease

Akinori Nakamura,[1,*] Pablo Cuesta,[1,2,3,*] Alberto Fernández,[2,4] Yutaka Arahata,[5,6] Kaori Iwata,[1] Izumi Kuratsubo,[6] Masahiko Bundo,[1,5] Hideyuki Hattori,[5] Takashi Sakurai,[5] Koji Fukuda,[5] Yukihiko Washimi,[5] Hidetoshi Endo,[5] Akinori Takeda,[5] Kersten Diers,[7] Ricardo Bajo,[2] Fernando Maestú,[2,8] Kengo Ito[1,5,6] and Takashi Kato[1,5]

*These authors contributed equally to this work.

Biomarkers useful for the predementia stages of Alzheimer's disease are needed. Electroencephalography and magnetoencephalography (MEG) are expected to provide potential biomarker candidates for evaluating the predementia stages of Alzheimer's disease. However, the physiological relevance of EEG/MEG signal changes and their role in pathophysiological processes such as amyloid-β deposition and neurodegeneration need to be elucidated. We evaluated 28 individuals with mild cognitive impairment and 38 cognitively normal individuals, all of whom were further classified into amyloid-β-positive mild cognitive impairment ($n = 17$, mean age 74.7 ± 5.4 years, nine males), amyloid-β-negative mild cognitive impairment ($n = 11$, mean age 73.8 ± 8.8 years, eight males), amyloid-β-positive cognitively normal ($n = 13$, mean age 71.8 ± 4.4 years, seven males), and amyloid-β-negative cognitively normal ($n = 25$, mean age 72.5 ± 3.4 years, 11 males) individuals using Pittsburgh compound B-PET. We measured resting state MEG for 5 min with the eyes closed, and investigated regional spectral patterns of MEG signals using atlas-based region of interest analysis. Then, the relevance of the regional spectral patterns and their associations with pathophysiological backgrounds were analysed by integrating information from Pittsburgh compound B-PET, fluorodeoxyglucose-PET, structural MRI, and cognitive tests. The results demonstrated that regional spectral patterns of resting state activity could be separated into several types of MEG signatures as follows: (i) the effects of amyloid-β deposition were expressed as the alpha band power augmentation in medial frontal areas; (ii) the delta band power increase in the same region was associated with disease progression within the Alzheimer's disease continuum and was correlated with entorhinal atrophy and an Alzheimer's disease-like regional decrease in glucose metabolism; and (iii) the global theta power augmentation, which was previously considered to be an Alzheimer's disease-related EEG/MEG signature, was associated with general cognitive decline and hippocampal atrophy, but was not specific to Alzheimer's disease because these changes could be observed in the absence of amyloid-β deposition. The results suggest that these MEG signatures may be useful as unique biomarkers for the predementia stages of Alzheimer's disease.

1 Department of Clinical and Experimental Neuroimaging, National Center for Geriatrics and Gerontology, Obu, 474-8511, Japan
2 Laboratory of Cognitive and Computational Neuroscience, Center for Biomedical Technology, Complutense University of Madrid and Technical University of Madrid, Madrid, 28223, Spain
3 Electrical Engineering and Bioengineering Lab, Department of Industrial Engineering, University of La Laguna, Tenerife, 38200, Spain
4 Department of Psychiatry, Faculty of Medicine, Complutense University of Madrid, Madrid, 28040, Spain
5 National Hospital for Geriatric Medicine, National Center for Geriatrics and Gerontology, Obu, 474-8511, Japan
6 Innovation Center for Clinical Research, National Center for Geriatrics and Gerontology, Obu, 474-8511, Japan
7 Department of Psychology, Technische Universität Dresden, Dresden, 01069, Germany
8 Department of Basic Psychology II, Complutense University of Madrid, Madrid, 28223, Spain

Received February 20, 2017. Revised November 26, 2017. Accepted January 6, 2018. Advance Access publication March 7, 2018

Correspondence to: Akinori Nakamura, MD, PhD
Department of Clinical and Experimental Neuroimaging, Center for Development of Advanced Medicine for Dementia, National Center for Geriatrics and Gerontology, 7-430, Morioka-cho, Obu, Aichi 474-8511, Japan
E-mail: nakamura@ncgg.go.jp

Keywords: Alzheimer's disease continuum; magnetoencephalography; resting state; regional power spectrum; amyloid imaging

Abbreviations: AAL = Automated Anatomical Labeling; CBPT = cluster-based permutation tests; CDR = Clinical Dementia Rating; CN(p/n) = cognitively normal (positive/negative amyloid-β deposition); MCI(p/n) = mild cognitive impairment (positive/negative amyloid-β deposition); MEG = magnetoencephalography; PiB = Pittsburgh compound B; SUVR = standardized uptake value ratio; VSRAD = voxel-based specific regional analysis system for Alzheimer's disease

Introduction

Alzheimer's disease is the most common neurocognitive disorder, with an estimated prevalence of ∼60–70% of the 47.5 million people with dementia world-wide (http://www.who.int/mediacentre/factsheets/fs362/en/). Recent disease-modifying clinical trials for Alzheimer's disease (Sperling *et al.*, 2014; Sevigny *et al.*, 2016) have emphasized the importance of early intervention in the predementia phases, which are categorized as mild cognitive impairment (MCI) and preclinical Alzheimer's disease stages in the diagnostic criteria of the National Institute on Aging and the Alzheimer's Association (NIA-AA) (Albert *et al.*, 2011; McKhann *et al.*, 2011; Sperling *et al.*, 2011). Therefore, the registration of individuals with predementia stages in global platforms aiming to facilitate clinical trials such as the global Alzheimer's platform (Cummings *et al.*, 2016) and the European Prevention of Alzheimer's Dementia (Ritchie *et al.*, 2016) has become the most recent global trend. However, as MCI manifests as a heterogeneous clinical status in which the clinical outcome is considerably variable (Larrieu *et al.*, 2002), identification of MCI individuals with biomarker evidence of Alzheimer's disease is crucial (Jack *et al.*, 2016; Wolz *et al.*, 2016). Such individuals are termed 'MCI due to Alzheimer's disease' (Albert *et al.*, 2011) by the NIA-AA criteria, or 'prodromal Alzheimer's disease' by the International Working Group on Alzheimer's disease (Dubois *et al.*, 2010, 2014). Biomarker information is more crucial to identify individuals in the preclinical stages of Alzheimer's disease who are cognitively asymptomatic but who also have evidence of amyloid-β deposition in the brain.

Biomarkers for Alzheimer's disease are important not only for identifying these high-risk individuals, but also for assessing the disease status or understanding the pathophysiological processes of disease progression. Amyloid-β deposition is the earliest pathognomonic signature of Alzheimer's disease, which starts decades before the actual onset of Alzheimer's disease (Morris, 2005; Bateman *et al.*, 2012; Villemagne *et al.*, 2013). Thus, biomarkers for amyloid-β deposition, such as amyloid-PET imaging signatures or decreased amyloid-$\beta_{1\text{-}42}$ and amyloid-$\beta_{1\text{-}42}$/amyloid-$\beta_{1\text{-}40}$ ratio in the CSF, are considered to be the most 'upstream' markers in the pathological cascade of Alzheimer's disease (Jack *et al.*, 2013). However, amyloid-β deposition does not necessarily represent progression to Alzheimer's disease, as many subjects with abundant amyloid-β deposition are able to live their natural lifespan cognitively intact (Snowdon, 1997). Therefore, identification of downstream biomarkers that can act as surrogate markers of disease progression is also important. These markers include the CSF concentrations of total tau and phosphorylated tau (Blennow *et al.*, 2010), tau-PET imaging markers (Maruyama *et al.*, 2013; Harada *et al.*, 2016), reduced glucose metabolism predominantly in the posterior cingulate, precuneus, and temporo-parietal cortices as measured by fluorodeoxyglucose (FDG)-PET (Drzezga *et al.*, 2003; Anchisi *et al.*, 2005; Mosconi, 2005), brain atrophy in the medial temporal area as assessed by structural MRI (Risacher *et al.*, 2009; Chételat *et al.*, 2012; Doré *et al.*, 2013), and accelerated cognitive decline (Storandt *et al.*, 2009; Lim *et al.*, 2014*b*).

EEG and magnetoencephalography (MEG) are expected to be useful for providing unique biomarker candidates (Stomrud *et al.*, 2010; Fernández *et al.*, 2013; López *et al.*, 2016), as they are direct measures of primary neural activity and have very fine temporal resolution (in the order of milliseconds). Moreover, their non-invasive nature allows for repeated measurements to monitor the disease status or to evaluate the effects of intervention. Patients with Alzheimer's disease and MCI generally show slowing of oscillatory brain activity (Stam, 2010; Lizio *et al.*, 2011; López *et al.*, 2014*b*; Engels *et al.*, 2016), and this slowing is associated with several factors such as cognitive status, risk of progression to dementia (Fernández *et al.*, 2006*b*; Prichep, 2007; López *et al.*, 2016), hippocampal atrophy (Fernández *et al.*, 2003), hypometabolism (Rodriguez *et al.*, 1998), CSF tau levels (Jelic *et al.*, 1998; Stomrud *et al.*, 2010; Kramberger *et al.*, 2013), *APOE4* genotype (Lehtovirta *et al.*, 1996; de Waal *et al.*, 2013; Cuesta *et al.*, 2014), and low cholinergic activity (Riekkinen and Sirviö, 1990). However, the usefulness of EEG/MEG characteristics as biomarkers for the evaluation of predementia stages of Alzheimer's disease is not yet fully established. One main reason is that only a few studies of predementia stages of Alzheimer's disease have been performed in which EEG/MEG was combined with amyloid-β biomarker information (Jelic *et al.*, 1998; Stomrud *et al.*, 2010; Kramberger *et al.*, 2013; Gouw *et al.*,

2017; Nakamura *et al.*, 2017). Therefore, the main objective of this study was to explore potential electrophysiological signatures that may act as surrogate markers of the pathophysiological changes that occur in the predementia stages of Alzheimer's disease. Further, we investigated the relevance of these biomarker candidates to their pathophysiological backgrounds by combining MEG data with amyloid-β biomarker data obtained using Pittsburgh compound B (PiB)-PET, downstream markers for neurodegeneration obtained using FDG-PET, and structural MRI.

Accordingly, we analysed regional spectral patterns of resting state MEG signals in 17 amyloid-β-positive individuals with MCI (MCIp), 11 amyloid-β-negative individuals with MCI (MCIn), 13 amyloid-β-positive cognitively normal (CNp) individuals, and 25 amyloid-β-negative CN individuals (CNn). To understand the characteristics of potential MEG signatures, we first explored the effects of amyloid-β deposition (amyloid-β positive versus amyloid-β negative) and clinical status (MCI versus CN), and their interaction by means of a two-way design. Second, we performed group-wise comparisons to further extract group-specific characteristics. Further, relationships between the MEG power markers and pathophysiological processes, including cognitive decline, regional glucose metabolism, and grey matter volume, were analysed. Through these assessments, we separately identified MEG signatures that were (i) related to amyloid-β deposition; (ii) related to downstream pathophysiological changes within the Alzheimer's disease continuum; and (iii) non-specific changes related to general cognitive decline or neurodegeneration.

Materials and methods

Participants

This investigation was a part of the Multimodal Neuroimaging for Alzheimer's disease Diagnosis (MULNIAD) study, which is a prospective longitudinal study targeting normal ageing, MCI, and Alzheimer's disease that was conducted at the National Center for Geriatrics and Gerontology (NCCG) in Obu, Japan. All participants were native Japanese individuals who were recruited from among community-dwelling aged individuals or outpatients at the National Hospital for Geriatric Medicine, NCGG. The study was approved by the Ethics Committee of NCGG, and all participants provided written informed consent. The original sample comprised 33 patients with MCI and 68 cognitively normal (CN) individuals. Based on visual ratings of PiB-PET imaging (see below), these individuals were classified into the amyloid-β-positive MCI (MCIp; $n = 21$), amyloid-β-negative MCI (MCIn; $n = 12$), amyloid-β-positive CN (CNp; $n = 13$), and amyloid-β-negative CN (CNn; $n = 55$) subgroups. Of these, four MCIp, one MCIn, and five CNn subjects were excluded because of significantly noisy MEG recordings. Because the CNn group had a significantly lower mean age compared to the other groups, we selected 25 CNn subjects who were age-, sex-, and education level-matched (with the other groups). Finally, we analysed 17 MCIp, 11 MCIn, 13 CNp, and 25 CNn subjects in this study (Table 1). To define the CN and MCI individuals, we followed the inclusion criteria of the Alzheimer's Disease Neuroimaging Initiative 2 study (http://adni.loni.usc.edu) (Supplementary material).

All participants underwent a comprehensive battery of neuropsychological tests and neuroimaging assessments including PiB-PET, FDG-PET, structural MRI, and MEG. All examinations were carried out within ~1 month of each other.

PiB-PET

Image acquisition

3D PET imaging for 50–70 min after intravenous injection of 555 ± 185 MBq ^{11}C-PiB was carried out using a PET CT camera, Biograph True V (Siemens Healthcare). X-ray CT was performed before PET imaging for attenuation correction.

Visual rating and classification

Visual rating of PiB-PET images was conducted according to the previously described protocol (Kaneko *et al.*, 2014), which followed the method reported by Rabinovici *et al.* (2011). This was used for classification of participants into amyloid-β-positive (CNp and MCIp) and amyloid-β-negative (CNn and MCIn) groups (Supplementary material).

Quantitative image analysis

Standardized uptake value ratio (SUVR) images were generated individually using the Automated Anatomical Labeling (AAL) atlas (Tzourio-Mazoyer *et al.*, 2002). As the representative measure of the quantitative amyloid-β burden, the mean cortical PiB-SUVR was obtained by averaging the SUVRs of the frontal, parietal, and temporal regions of interest from the AAL atlas. The PiB-SUVR images were spatially smoothed using a Gaussian kernel filter with a full-width at half-maximum of 8 mm. Whole-brain voxel-wise regression analysis for MEG power data was performed with these smoothed images using the Statistical Parametric Mapping (SPM8, Wellcome Trust Centre for Neuroimaging, University College, London, UK) software suite (Supplementary material).

FDG-PET

Image acquisition

Using the same scanner and attenuation correction method as used for PiB-PET, ^{18}F-FDG-PET images were obtained. Whole-brain voxel-wise regression analysis for the MEG power data with the FDG-PET images was performed using SPM8 (Supplementary material).

MRI

Image acquisition

High-resolution 3D T_1-weighted images were acquired using a Trio 3 T scanner (Siemens) and used for volumetric analysis (Supplementary material). T_2-weighted and fluid attenuated inversion recovery images were also acquired to assess brain lesions.

Table 1 Participant demographics

	CNp (n = 13)	CNn (n = 25)	MCIp (n = 17)	MCIn (n = 11)	Statistics (P-value)
Sex (M / F)	7/6	11/14	9/8	8/3	0.47
Age (y)	71.8 ± 4.4	72.5 ± 3.4	74.7 ± 5.4	73.8 ± 8.8	0.43
Education (y)	12 ± 3	12 ± 3	11 ± 3	12 ± 3	0.59
MMSE	28.77 ± 1.09	28.60 ± 1.38	26.29 ± 1.65	26.64 ± 2.87	<0.001
ADAS-Jcog	5.74 ± 2.19	5.87 ± 2.67	9.09 ± 2.04	9.35 ± 3.28	<0.001
LM1	20.77 ± 7.25	20.36 ± 6.40	11.47 ± 4.99	12.00 ± 6.26	<0.001
LM2	16.23 ± 6.85	16.24 ± 6.17	4.18 ± 5.14	7.00 ± 7.20	<0.001
CDR	0	0	0.5	0.5	-
CDR-SOB	0.04 ± 0.14	0.08 ± 0.19	1.85 ± 1.03	1.73 ± 1.19	<0.001
GDS	2.00 ± 1.29	2.08 ± 1.63	2.41 ± 1.66	2.82 ± 1.66	0.58
APOEε4 (%)	4/13 (30.8)	4/25 (16.0)	13/17 (76.5)	0/11 (0.0)	<0.001
PiB-mcSUVR	1.44 ± 0.19	1.13 ± 0.06	1.89 ± 0.25	1.13 ± 0.06	<0.001
VSRAD score	0.54 ± 0.18	0.69 ± 0.42	1.34 ± 0.62	1.14 ± 0.67	<0.001

Values are presented as mean ± SD. Statistical analyses were performed using the chi square test (sex, APOEε4) and one-way ANOVA (others).
ADAS-Jcog = Alzheimer's Disease Assessment Scale-Cognitive Component-Japanese version; APOEε4 = positive for apolipoprotein E ε4; CDR = Clinical Dementia Rating; CDR-SOB = Sum of Boxes of CDR; GDS = Geriatric Depression Scale; LM1/LM2 = Logical Memory I/II from the Wechsler Memory Scale–Revised (paragraphs A and B); MMSE = Mini-Mental State Examination; PiB-mcSUVR = mean cortical SUVR of PiB-PET; VSRAD score = the degree of grey matter atrophy of the medial temporal region using a z-score computed by VSRAD (also see Supplementary Fig. 1).

Volumetric analysis

Atrophy in the medial temporal region, including the hippocampus, head to tail of the hippocampus, and amygdala, was quantitatively assessed using the Voxel-based Specific Regional Analysis System for Alzheimer's Disease (VSRAD® advance, Eisai Co., Ltd., Tokyo, Japan) software, which is based on SPM8 and Diffeomorphic Anatomical Registration Through Exponentiated Lie Algebra (DARTEL; Matsuda *et al.*, 2012; Matsuda, 2013) (Supplementary material).

The spatially normalized and grey matter-segmented images created by VSRAD were also used for whole-brain voxel-wise regression analysis using SPM8, and the associations between the MEG power values and grey matter volume were estimated.

MEG

Data acquisition

The MEG measurements were performed using a 306-channel whole-head MEG system (Vectorview, ElektaNeuromag) located in a magnetically shielded room at the NCGG. Participants sat comfortably on a chair with their eyes closed, and resting state MEG signals were measured for 5 min with a sampling rate of 1000 Hz (online bandpass anti-alias filtering at 0.1–330 Hz) (Supplementary material). The arousal level of each subject was monitored with a video camera (WV-CL934, Panasonic) and also checked via a conversation immediately following the measurement session. If a subject reported feeling sleepy during the session, we gave him/her sufficient time to feel more awake and performed the measurement again.

Computation of the power spectra

After data preprocessing (Supplementary material), at least 20 artefact-free fragments (trials) of continuous 4-s MEG signals (80 s of brain activity) were obtained from all participants, and 20 of these clean trials were randomly selected from each subject to equalize the number of trials. The time series was filtered using a broadband filter (1.4–55 Hz) with a Finite Impulse Response filter (order, 1500) designed with a Hanning window.

Using the realistic single-shell model with a 1-cm spacing grid (2455 nodes), source reconstruction was performed using a Linearly Constrained Minimum Variance Beamformer (Van Veen *et al.*, 1997) (Supplementary material).

The MEG power spectra of each node were computed for all artefact-free trials. A frequency-of-interest range from 1.5–55 Hz (in 0.5-Hz steps) was used. To obtain the average frequency content of each trial, we applied a multitaper method with discrete prolate spheroidal sequences as windowing functions and 1 Hz smoothing. Trials were averaged across subjects, obtaining a matrix with dimension: 2455 nodes × 108 frequency steps × 66 subjects. For each node, the relative power was calculated by normalizing with the total power over the 1.5- to 55-Hz range (Jelic *et al.*, 2000).

Design for data analyses

To separately detect MEG power spectral changes related to amyloid-β deposition and clinical status, the data were analysed in a two-way design that tested for the main effects of amyloid-β deposition (amyloid-β-positive groups versus amyloid-β-negative groups), clinical status (MCI groups versus CN groups), and their interaction. Also, group-wise comparisons were conducted to test for the effects of amyloid-β deposition within the CN groups (CNp versus CNn), and within the MCI groups (MCIp versus MCIn). In addition, the effects of clinical status were tested within the amyloid-β-positive groups (CNp versus MCIp), and within the amyloid-β-negative groups (CNn versus MCIn). It is well known that ageing strongly affects the MEG/EEG power spectrum (Rossini *et al.*, 2007), and thus, the analyses were conducted while adjusting for the effects of age using analysis of covariance (ANCOVA).

Region of interest-based analysis

The source-reconstructed MEG power data were first analysed by atlas-based region of interest analysis to visualize the

characteristics of the regional spectral patterns as waveforms. We set 10 representative regions of interest by referring to the AAL atlas (Tzourio-Mazoyer *et al.*, 2002), so that the whole cortical mantle was roughly covered. Five regions of interest were related to the default mode network (Buckner *et al.*, 2008), because amyloid-β first accumulates in areas associated with the default mode network (Mintun *et al.*, 2006), and glucose hypometabolism in the posterior hub of the default mode network is an established marker for disease progression (Small *et al.*, 2000). Accordingly, the 10 regions of interest were: frontal medial cortex, anterior cingulate cortex, left and right frontal cortices, left and right temporal cortices, left and right inferior parietal lobules, precuneus/posterior cingulate cortex, and occipital cortex (Supplementary Table 1).

For these regions of interest, the effects of amyloid-β deposition and clinical status were visualized in a spatio-frequential domain by plotting the *F*-values, which were computed by two-way and group-wise ANCOVAs for each frequency step (0.5 Hz) while adjusting for the effects of age.

Node-based whole-brain analysis

The region of interest-based analyses were performed mainly for visualization purposes, whereas actual statistical analyses were conducted on node-based whole-brain analysis.

The source template with 2455 nodes in a 1-cm spacing grid was segmented into 72 AAL (Tzourio-Mazoyer *et al.*, 2002) regions of interest that included all AAL regions of interest but excluded the cerebellum, basal ganglia, thalamus, amygdala, insula, and olfactory cortices using the AAL version made for SPM8 included in Fieldtrip software (Oostenveld *et al.*, 2011). The 72 regions of interest included 1137 of the original 2455 nodes. The source-reconstructed MEG power data were analysed with a matrix of 1137 nodes × 108 frequency steps × 66 subjects.

To overview spatio-frequential topography of the effects of amyloid-β deposition and clinical status, *F*-values for the two-way and group-wise ANCOVAs were computed at each of the 1137 nodes for each frequency and overlaid on the standard brain of the Montreal Neurological Institute.

Significant clusters, which showed significant effects of amyloid-β deposition or clinical status, were explored using cluster-based permutation tests (CBPT) (Maris and Oostenveld, 2007) performed over the 1137 nodes, using Fieldtrip toolbox (Oostenveld *et al.*, 2011). To enhance the frequential resolution, the results of the above spatio-frequential *F*-value maps as well as the region of interest-based analyses were used to define specific frequency ranges of interest for each candidate. Within each classical frequency band [i.e. delta (2–4 Hz), theta (4–8 Hz), and alpha (8–12 Hz)], we defined three frequency steps bands centred at the frequency with the largest effect. Then, whole-brain power spectral data were averaged within the corresponding frequency band and submitted to the CBPT. The CBPT were executed with 10 000 repetitions to create a null distribution for each comparison. This null distribution was obtained by shuffling the original values and performing a two-way or one-way ANCOVA test with age as a confounding covariate for testing the two-way or group-wise comparisons, respectively. The maximum statistic at each repetition was kept for the permutation distribution. The CBPT *P*-value represents the proportion of the permutation distribution with *F*-values greater than or equal to the *F*-value of the original data. The alpha level was set to 0.05 for the CBPT *P*-value. To enhance the spatial resolution of the results, the critical value for the clusters configuration was fixed to 0.01. Only those clusters that were retained after the CBPT were used for subsequent analyses as potential 'MEG power markers'. Power values of all nodes included in a cluster were averaged individually and used as power marker values for the subsequent correlation, regression, or receiver operating characteristic (ROC) analyses.

Correlations between the MEG power markers and the mean cortical PiB-SUVR values, VSRAD scores, or the scores for the cognitive tests were assessed by multiple correlation analysis using age as a confounding covariate.

The ROC analyses were used to evaluate the performances of MEG power markers to predict amyloid-β positivity or negativity (Supplementary material). ROC analyses were performed, adjusting for the effects of age as follows: for each MEG power marker, a predictive formula that included age as a confounder was built by using binomial logistic regression analysis. Then, the predictive values were computed and used for the age-adjusted ROC analyses.

Statistical analyses were performed using Matlab R2009b (The Mathworks Inc., Natick, MA, USA) and SPSS v. 21 (IBM, Armonk, NY, USA) software. All tests were two-tailed, and the significance level threshold was set at $P < 0.05$ unless explicitly stated otherwise.

Results

Participant demographics

The demographic characteristics of the participants are shown in Table 1. No differences were present in sex, age, or educational level among the four groups. Overall, performance on the neuropsychological tests was significantly lower in the MCI groups than in the CN groups, except for the Geriatric Depression Scale score. The proportion of *APOE-ε4* carriers was significantly higher in the MCIp group compared to all the other groups. The mean cortical SUVR of PiB-PET values was significantly higher in the MCIp group compared to all the other groups, and the CNp group showed a higher mean cortical PiB-SUVR value than the MCIn and CNn groups. The VSRAD scores were significantly higher (implying a higher level of atrophy) in the MCIn group than in the CNn group ($P = 0.019$), and in the MCIp group than in the CNp group ($P < 0.001$; Supplementary Fig. 1).

General profile of the regional power spectra

To provide an overview of the power-frequency profile of the MEG resting state signals for each group, the relative power spectra and their subtractions of two-way comparisons were plotted at 10 representative regions of interest (Fig. 1A). In the frequency range below 7 Hz, which corresponds to the classical description of theta and delta bands, the MCI groups generally showed larger power values than the CN groups in all regions of interest

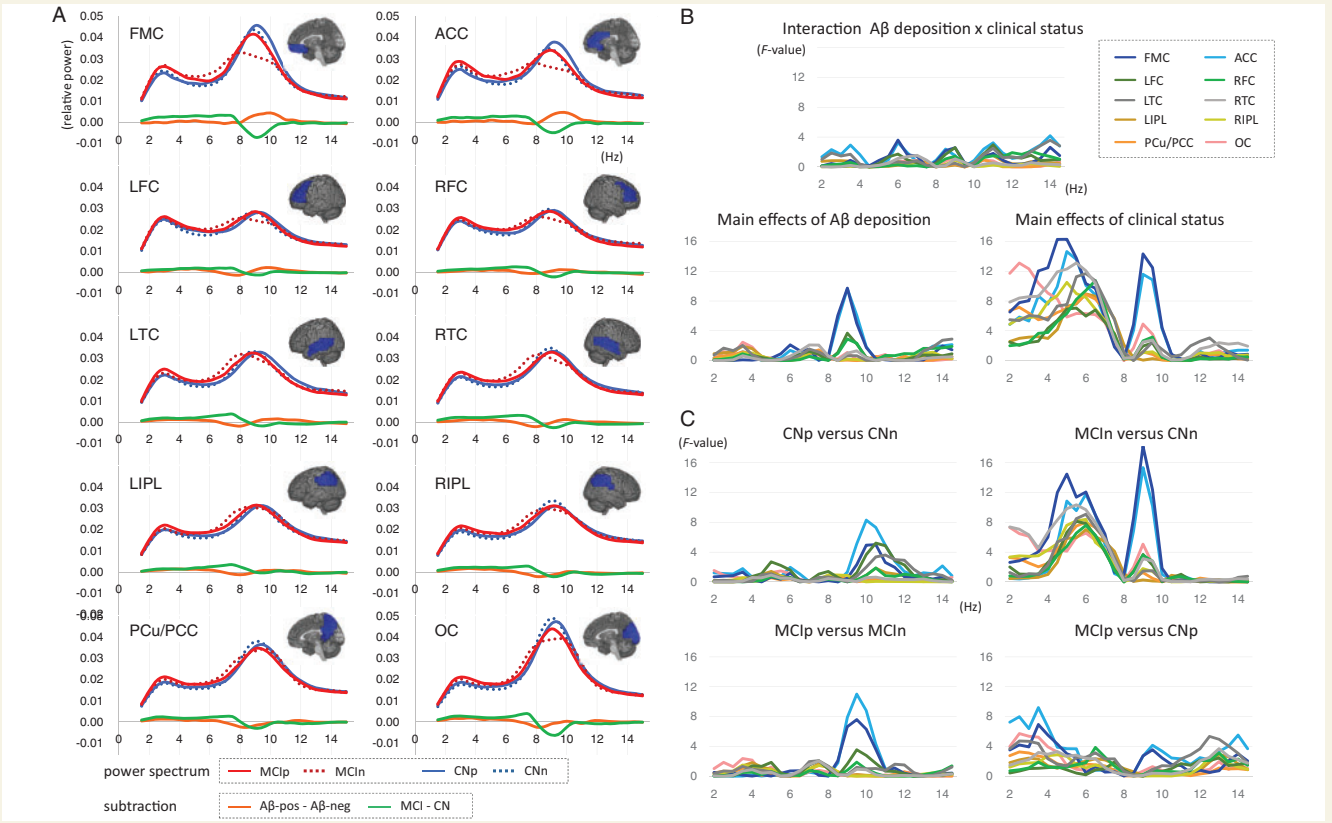

Figure 1 General profiles of the power spectra at each region of interest. (**A**) Waveforms of the power spectra for each group and their two-way subtractions (amyloid-β-positive groups − amyloid-β-negative groups, and MCI groups − CN groups). Brain images show the shape of the regions of interest. ACC = anterior cingulate cortex; FMC = frontal medial cortex; LFC and RFC = left and right frontal cortices; LIPL and RIPL = left and right inferior parietal lobules; LTC and RTC = left and right temporal cortices; OC = occipital cortex; PCu/PCC = precuneus/posterior cingulate cortex; see also Supplementary Table 1. (**B**) *F*-values for the main effects of amyloid-β deposition and clinical status and their interactions, plotted by frequency. The *F*-values were adjusted for the effects of age. Each region of interest profile is coded in a different colour. (**C**) *F*-values for the group-wise comparisons.

(Fig. 1A, green lines). On the other hand, in the frequency range 8–11 Hz, which corresponds to the classical alpha band, the amyloid-β-positive groups showed stronger power compared with the amyloid-β-negative groups in the medial frontal regions of interest (frontal medial cortex and anterior cingulate cortex) (Fig. 1A, orange lines). In particular, the CNp group showed the strongest alpha power among all four groups in these regions of interest, whereas the MCIn group was the weakest. In addition, the alpha power in these regions of interest was weaker in the MCI groups than the CN groups.

MEG signatures showing effects of amyloid-β deposition and clinical status

To visualize the effects of amyloid-β deposition and clinical status in a spatio-frequency domain, *F*-values of the two-way and group-wise ANCOVAs at each of the representative regions of interest were plotted (Fig. 1B and C). In the two-way analyses, stronger main effects of amyloid-β deposition were found in the prefrontal regions of interest (frontal medial cortex and anterior cingulate cortex) at a frequency range peaking around 9 Hz (Fig. 1B, bottom left). In contrast, stronger main effects of clinical status were found in most regions of interest in a frequency range lower than 7 Hz (Fig. 1B, bottom right). In addition, significant main effects of clinical status were found in the prefrontal regions of interest at a peak frequency ∼9 Hz. We found no prominent interaction between amyloid-β deposition and clinical status (Fig. 1B, top). In the group-wise analyses for effects of amyloid-β deposition, both within the CN groups (CNp versus CNn) and within the MCI groups (MCIp versus MCIn), comparisons showed prominent effects in the prefrontal regions of interest at peak frequencies of 10 Hz (Fig. 1C, top left) and 9 Hz (Fig. 1C, bottom left), respectively. For the group-wise effects of clinical status, the spatio-frequency profiles appeared quite different when comparing the amyloid-β-positive groups (MCIp versus CNp) and the amyloid-β-negative groups (MCIn versus CNn). Within the amyloid-β-negative group comparisons, the spatio-frequency

Table 2 Significant MEG power markers

	Comparisons	Regions	Classical band	Peak frequency	Power (SD)	Power (SD)	ANCOVA *F* value	*P*- value*	η_p^2
Effects of amyloid-β deposition									
Main effects					**Aβp**	**Aβn**			
	Aβp > Aβn	Prefrontal	Alpha		0.036(0.008)	0.032(0.006)	11.325	0.001	0.157
Group effects					**CNp**	**CNn**			
Within CN	CNp > CNn	Prefrontal	Alpha	10.5 Hz	0.029(0.006)	0.023(0.005)	10.821	0.002	0.236
					MCIp	**MCIn**			
Within MCI	MCIp > MCIn	Prefrontal	Alpha	9 Hz	0.037(0.007)	0.028(0.005)	13.318	0.001	0.348
Effects of clinical status									
Main effects					**MCI**	**CN**			
	MCI > CN	Posterior	Delta	2.5 Hz	0.019(0.004)	0.017(0.003)	12.340	0.001	0.168
	MCI > CN	Global	Theta	4.5 Hz	0.020(0.004)	0.018(0.003)	12.529	0.001	0.170
	CN > MCI	Prefrontal	Alpha	9.5 Hz	0.031(0.007)	0.035(0.006)	13.905	0.000	0.186
Group effects					**MCIn**	**CNn**			
Within Aβn	MCIn > CNn	Occipitotemporal	Delta	2.5 Hz	0.019(0.005)	0.016(0.003)	18.473	0.000	0.359
	MCIn > CNn	Occipitotemporal	Theta	4.5 Hz	0.020(0.005)	0.016(0.003)	16.021	0.000	0.327
	MCIn > CNn	Prefrontal	Theta	5.5 Hz	0.022(0.006)	0.018(0.003)	13.051	0.001	0.283
	CNn > MCIn	Prefrontal	Alpha	9 Hz	0.028(0.005)	0.038(0.007)	17.601	0.000	0.348
					MCIp	**CNp**			
Within Aβp	MCIp > CNp	Occipital	Delta	3 Hz	0.021(0.003)	0.017(0.004)	10.757	0.003	0.285
	MCIp > CNp	Prefrontal	Delta	3.5 Hz	0.027(0.005)	0.022(0.004)	11.278	0.002	0.295

*Statistical test using ANCOVA adjusted for age.
Aβn/p = amyloid-β-negative/positive.

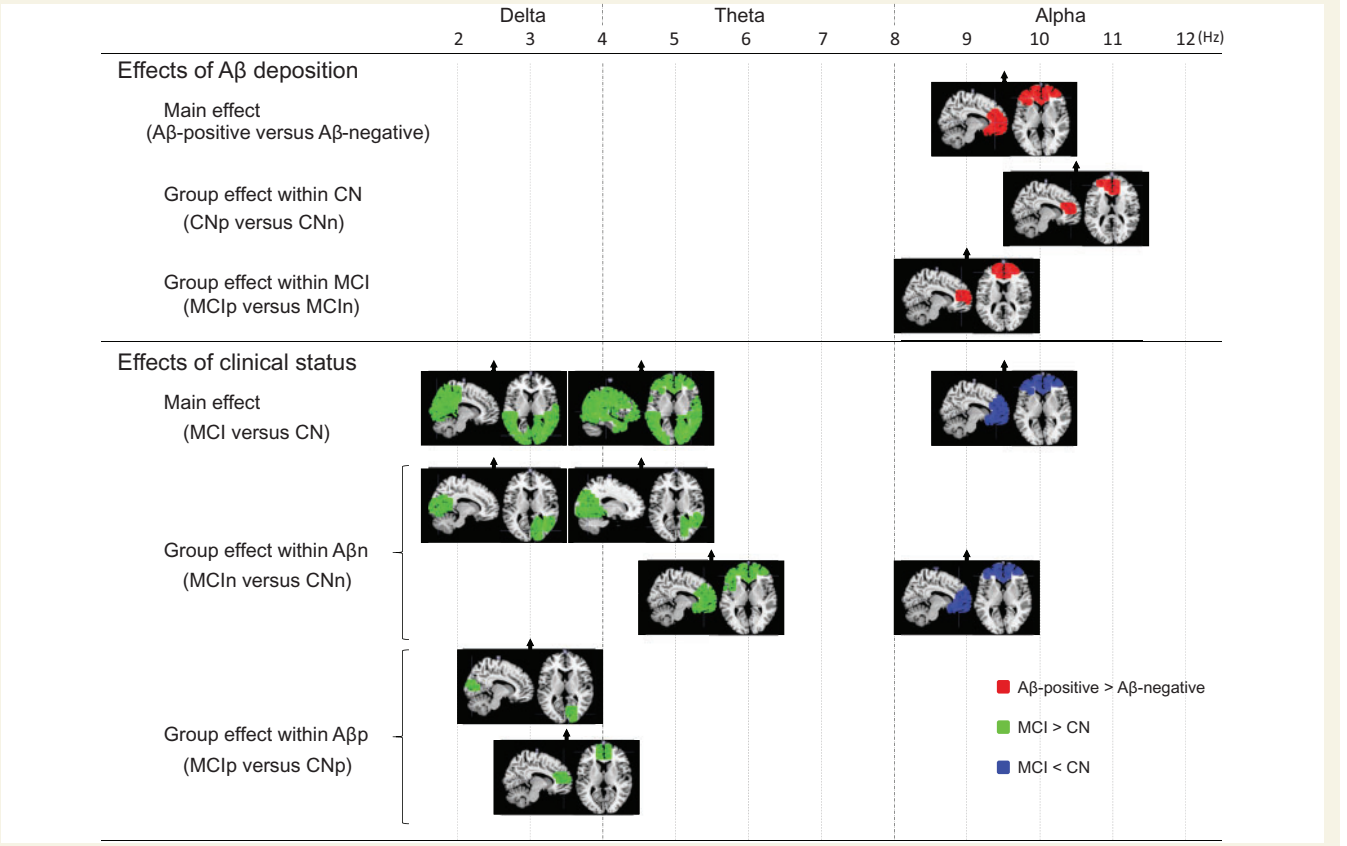

Figure 2 MEG power markers representing the effects of amyloid-β (Aβ) deposition and clinical status. The shape of each cluster is overlapped on the standard brain of the Montreal Neurological Institute. Each arrow indicates the peak frequency where the maximum effect was detected. The red colour indicates that the amyloid-β-positive groups showed larger power than the amyloid-β-negative groups, the green colour indicates larger power in the MCI groups than the CN groups, and the blue colour indicates the opposite.

profile was similar to that observed in the two-way analyses, showing stronger effects at peak frequencies around 5–6 Hz in all regions of interest and stronger effects around 9 Hz in the frontal regions of interest (Fig. 1C, top right). In contrast, the amyloid-β-positive group comparisons demonstrated stronger effects of the clinical status in the prefrontal and occipital regions of interest at peak frequencies around 2–4 Hz (Fig. 1C, bottom right).

These region of interest-based findings were confirmed with whole-brain analyses that computed *F*-values for each node involved in the whole cortical regions. Topographical maps of *F*-values at each frequency, which are shown in Supplementary Fig. 2A–C, demonstrated similar spatio-frequency profiles as the region of interest-based analyses for each effect related to amyloid-β deposition or clinical status.

Finally, we extracted statistically significant clusters that showed significant effects of amyloid-β deposition or clinical status, using the CBPT (Maris and Oostenveld, 2007) applied for the node-level whole-brain analysis. These clusters are listed in Table 2, and were used for the subsequent analyses as potential MEG power markers. Accordingly, we identified 12 MEG power markers as shown in Fig. 2. Three markers represented the effects of amyloid-β deposition as alpha band power augmentation in the amyloid-β-positive groups compared with the amyloid-β-negative groups in the prefrontal regions. The centre frequencies were 9.5 Hz for the main effects, and 10.5 Hz and 9 Hz for the within-group effects in the CN and MCI groups, respectively (Fig. 2, red clusters). The other nine power markers represented the effects of clinical status as either a power increase in the MCI groups (MCI > CN) within the delta and theta bands (Fig. 2, green clusters), or an alpha power decrease in the MCI groups (Fig. 2, blue clusters). The power markers for the group effects within the amyloid-β-negative groups were similar to those observed in the main effects, and appeared to be a type of subset of the main effects. On the other hand, two power markers for the group effects of clinical status within the amyloid-β-positive groups were represented as a delta band power increase in the MCIp group in the occipital and medial prefrontal regions. Detailed anatomical correspondence between these MEG power marker clusters and the regions of interest of the AAL atlas are shown in Supplementary Table 2.

Links between MEG power markers and pathophysiological processes

Amyloid-β deposition

To assess the relevance of the MEG power markers to pathophysiological processes, including amyloid-β deposition, neurodegeneration, and cognitive decline, multiple correlation analyses between the MEG power marker values and cognitive/imaging scores were performed while adjusting for the effects of age (Table 3).

The three power markers that represented the effects of amyloid-β deposition as prefrontal alpha power augmentation did not show any significant correlations with cognitive scores

Table 3 Correlations between the MEG power markers and cognitive/imaging scores

	Regions	Classical band	Peak frequency Hz	Partial correlation (*r*) adjusted for age						
				mcSUVR	VSRAD	MMSE	ADAS-Jcog	LM1	LM2	CDR-SOB
Effect of amyloid-β deposition										
Main effects										
	Prefrontal	Alpha	9.5	0.138	−0.196	0.150	−0.234	0.116	0.142	−0.178
Group effects										
Within CN	Prefrontal	Alpha	10.5	0.412*	−0.210	0.009	−0.033	−0.031	0.014	0.039
Within MCI	Prefrontal	Alpha	9	0.468*	0.156	0.132	−0.085	−0.193	−0.168	0.110
Effect of clinical status										
Main effects										
	Posterior	Delta	2.5	0.150	0.352**	−0.382**	0.358**	−0.304*	−0.355**	0.449***
	Global	Theta	4.5	0.227	0.425***	−0.347**	0.360**	−0.351**	−0.425***	0.474***
	Prefrontal	Alpha	9.5	0.115	−0.215	0.174	−0.252*	0.143	0.174	−0.199
Group effects										
Within Aβn	Occipitotemporal	Delta	2.5	−0.023	0.497**	−0.493**	0.406*	−0.388*	−0.364*	0.589***
	Occipitotemporal	Theta	4.5	0.136	0.572***	−0.353*	0.419*	−0.327	−0.405*	0.497**
	Prefrontal	Theta	5.5	0.180	0.406*	−0.267	0.312	−0.267	−0.346*	0.444**
	Prefrontal	Alpha	9	−0.027	−0.213	0.304	−0.265	0.318	0.236	−0.497**
Within Aβp	Occipital	Delta	3	0.188	0.216	−0.386*	0.440*	−0.369*	−0.483**	0.493**
	Prefrontal	Delta	3.5	0.323	0.488**	−0.387*	0.410*	−0.389*	−0.447*	0.467*

Asterisks indicate statistically significant correlations: (*$P < 0.05$, **$P < 0.01$, ***$P < 0.001$). Aβn/p = amyloid-β-negative/positive ADAS-Jcog = Alzheimer's Disease Assessment Scale-Cognitive Component-Japanese version; APOEε4 = positive for apolipoprotein E ε4; CDR = Clinical Dementia Rating; CDR-SOB = Sum of Boxes of CDR; GDS = Geriatric Depression Scale; LM1/LM2 = Logical Memory I/II from the Wechsler Memory Scale–Revised (paragraphs A and B); MMSE = Mini-Mental State Examination; PiB-mcSUVR = mean cortical SUVR of PiB-PET; VSRAD score = the degree of grey matter atrophy of the medial temporal region using a z-score computed by VSRAD.

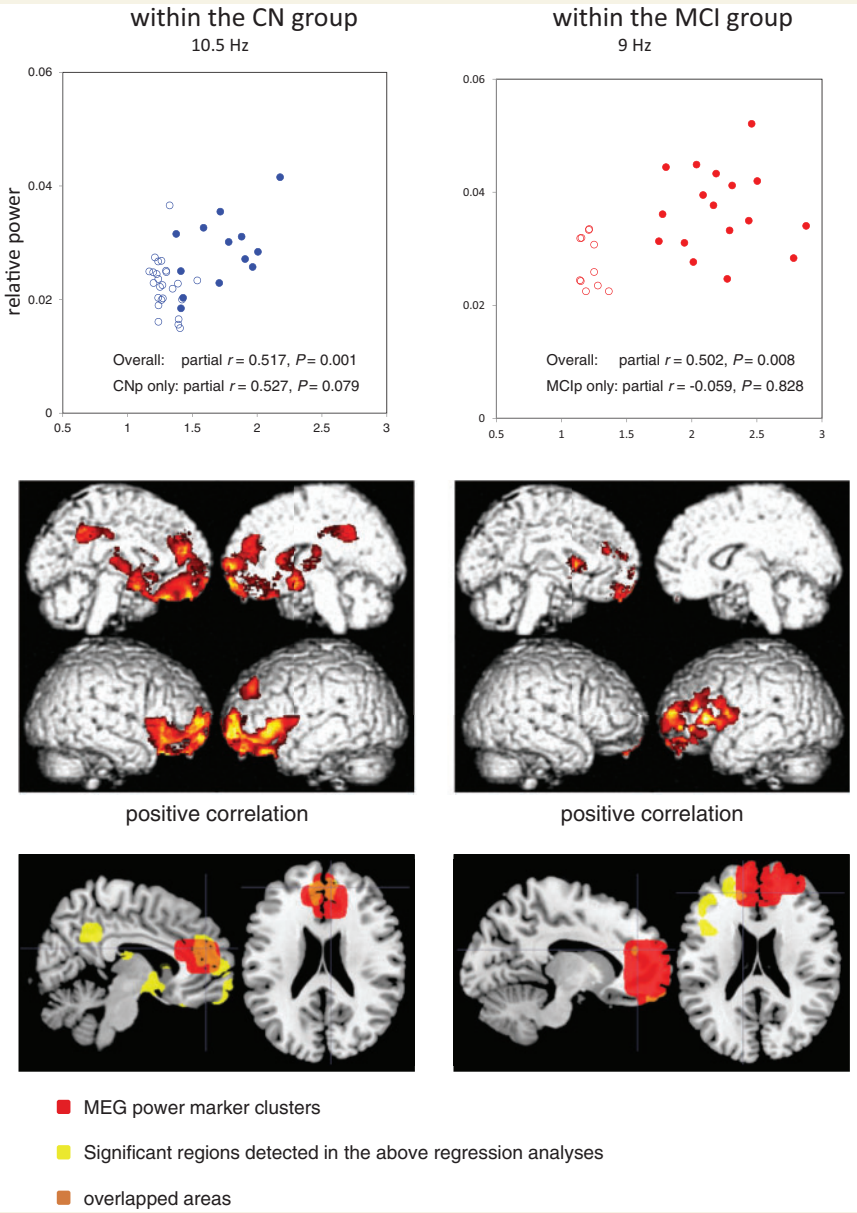

Figure 3 Relationships between the relative MEG power and regional amyloid-β deposition. *Top*: Scatter plots of the power marker values with local PiB-SUVR values, which were computed when limited within each power marker cluster, within the CN groups (*left*), and within the MCI groups (*right*). Closed circles indicate amyloid-β-positive individuals, and open circles indicate amyloid-β-negative individuals. Partial *r*-values represent correlation coefficients adjusted for the effects of age. The partial *r*-value was also computed by restricting the values within the amyloid-β-positive group for each CNp and MCIp. *Middle*: Whole-brain multiple regression analysis between PiB-PET SUVR images and power marker values adjusted for the effects of age. Significant clusters (FWE-corrected $P < 0.05$ at a height threshold of $P = 0.001$) are displayed. *Bottom*: Overlays of the cluster shape of MEG power markers (red) and significant regions detected in the above regression analyses (yellow). Overlapped areas are shown in orange.

such as the Mini-Mental State Examination, Alzheimer's Disease Assessment Scale-Cognitive Component-Japanese version (ADAS-Jcog), Logical Memory I/II from the Wechsler Memory Scale–Revised (LM1, LM2), and Clinical Dementia Rating-Sum of Boxes (CDR-SOB) scores, or with the quantitative measures of medial temporal atrophy as assessed with VSRAD scores (Table 3). Among them, however, two power markers showed group effects within CN and within MCI and demonstrated significant positive correlations with the mean cortical PiB-SUVR values with a partial $r = 0.412$ ($P = 0.011$) and 0.468 ($P = 0.014$), respectively (Table 3, mean cortical SUVR). The correlation coefficients became higher when the correlations were analysed against local PiB-SUVR values that were computed when limited within each power marker cluster. The partial r values for the within-CN and within-MCI markers were 0.517 ($P = 0.001$) and 0.502 ($P = 0.008$), respectively (Fig. 3, top). The results suggested that these power marker values are associated more

with local amyloid-β deposition than with global amyloid-β burden. In addition, correlations were also analysed with only the amyloid-β-positive groups (CNp and MCIp). Within the CNp group, the dose-dependent effect of local amyloid-β load on the alpha power augmentation was intermediately high (partial $r = 0.527$), although it did not reach significance ($P = 0.079$), whereas such an effect was not observed within the MCIp group (partial $r = -0.059$, $P = 0.828$).

To elucidate the topographical relationship between these power markers and cerebral amyloid-β deposition further, we conducted whole-brain regression analyses using PiB-SUVR images. The results demonstrated that the power marker values were significantly associated with amyloid-β deposition, mainly in the prefrontal regions (Fig. 3, middle). In particular, the within-CN power marker showed a close topographical relationship in the anterior cingulate and medial prefrontal cortices with local amyloid-β deposition (Fig. 3, bottom), suggesting that the link between the alpha power augmentation and local amyloid-β load in these regions is stronger in the CN groups compared with that in the MCI groups.

Neurodegeneration

In contrast, the nine MEG power markers, which represented the main effects or group effects of clinical status, were not significantly correlated with the mean cortical PiB-SUVR values (Table 3). However, all of them demonstrated significant correlations with at least one cognitive score, including the ADAS-Jcog, LM1, LM2, or CDR-SOB (Table 3). In particular, the low-frequency power markers (delta and theta) generally showed stronger correlations than the alpha-range power markers. All these low-frequency markers, except the within-amyloid-β-positive occipital delta marker, also demonstrated a significantly positive correlation with the VSRAD scores (Table 3), indicating that these power markers are associated with the degree of medial temporal atrophy.

To investigate the relevance of the power markers to neurodegenerative processes further, we conducted whole-brain voxel-wise regression analyses between the power marker values and regional grey matter volume using individual structural MRIs. Also, regression analyses between the power values and regional glucose metabolism were conducted using individual FDG-PET images. The power markers, which represented the main effects of clinical category in the posterior delta power (2.5 Hz) and global theta power (4.5 Hz), demonstrated that their power values were significantly negatively correlated with the grey matter volume in the hippocampal region [cluster level family wise error (FWE)-corrected $P < 0.05$] (Fig. 4A). Because the analyses were conducted based on whole-brain voxel-based morphometry, the results indicated that the relationship to the structural change was very specifically limited to the hippocampal volume. The prefrontal alpha power (9.5 Hz) did not show such correlations. The regression analyses of these power markers with FDG-PET images did not show any significant clusters.

Similarly, the power markers, which represented the group effects of clinical category within the amyloid-β-negative groups in the occipitotemporal delta (2.5 Hz) and theta (4.5 Hz) power, also demonstrated significant negative correlations with the hippocampal grey matter volume (Fig. 4B), whereas the prefrontal theta (5.5 Hz) and alpha (9 Hz) power did not show such correlations. These power markers did not show any significant associations with FDG-PET images.

Notably, the power marker, which represented the group effects of clinical category within the amyloid-β-positive groups in the prefrontal delta (3.5 Hz), demonstrated significantly negative correlations with the grey matter volume mainly in the entorhinal cortex (Fig. 4C). Further, the regression analysis of this marker with FDG-PET images showed a significant negative correlation with regional glucose metabolism in the precuneus and posterior cingulate cortices (Fig. 4D), indicating that increased medial prefrontal delta power was associated with Alzheimer's disease-type hypometabolism. The power marker in the occipital delta (3 Hz) did not show such relationships.

Discussion

In this study, we extracted several MEG power markers that represented either the effects of amyloid-β deposition or the effects of the clinical status. Further, this study disclosed the relevance of these power markers to pathophysiological processes, including amyloid-β deposition, neurodegeneration, and cognitive decline in detail. To the best of our knowledge, this is the first report that systematically identifies the regional spectral patterns of the spontaneous electromagnetic brain activity in MCI and CN subjects by combining MEG with multiple imaging modalities, including PiB-PET, FDG-PET, and structural MRI.

Effects of amyloid-β deposition on regional power spectra

The results demonstrated that the effects of amyloid-β deposition were manifested as the alpha power increment in prefrontal regions. This alpha augmentation was significantly correlated with amyloid-β burden in the same or adjacent prefrontal areas, and this topographical association was more evident within the CN group than within the MCI group. Several studies have shown that individuals in the predementia stages of Alzheimer's disease exhibit functional upregulation in the frontal areas of the brain. Using MEG, our group reported that functional connectivity between the anterior cingulate cortex and temporo-occipital regions in the alpha band become hypersynchronous in patients with progressive MCI who converted to Alzheimer's disease (López *et al.*, 2014*a*). The increased functional connectivity in the frontal areas was also reported using resting state functional MRI in individuals with amnestic MCI (Qi *et al.*, 2010) and in amyloid-β-positive CN elderly individuals (Mormino *et al.*,

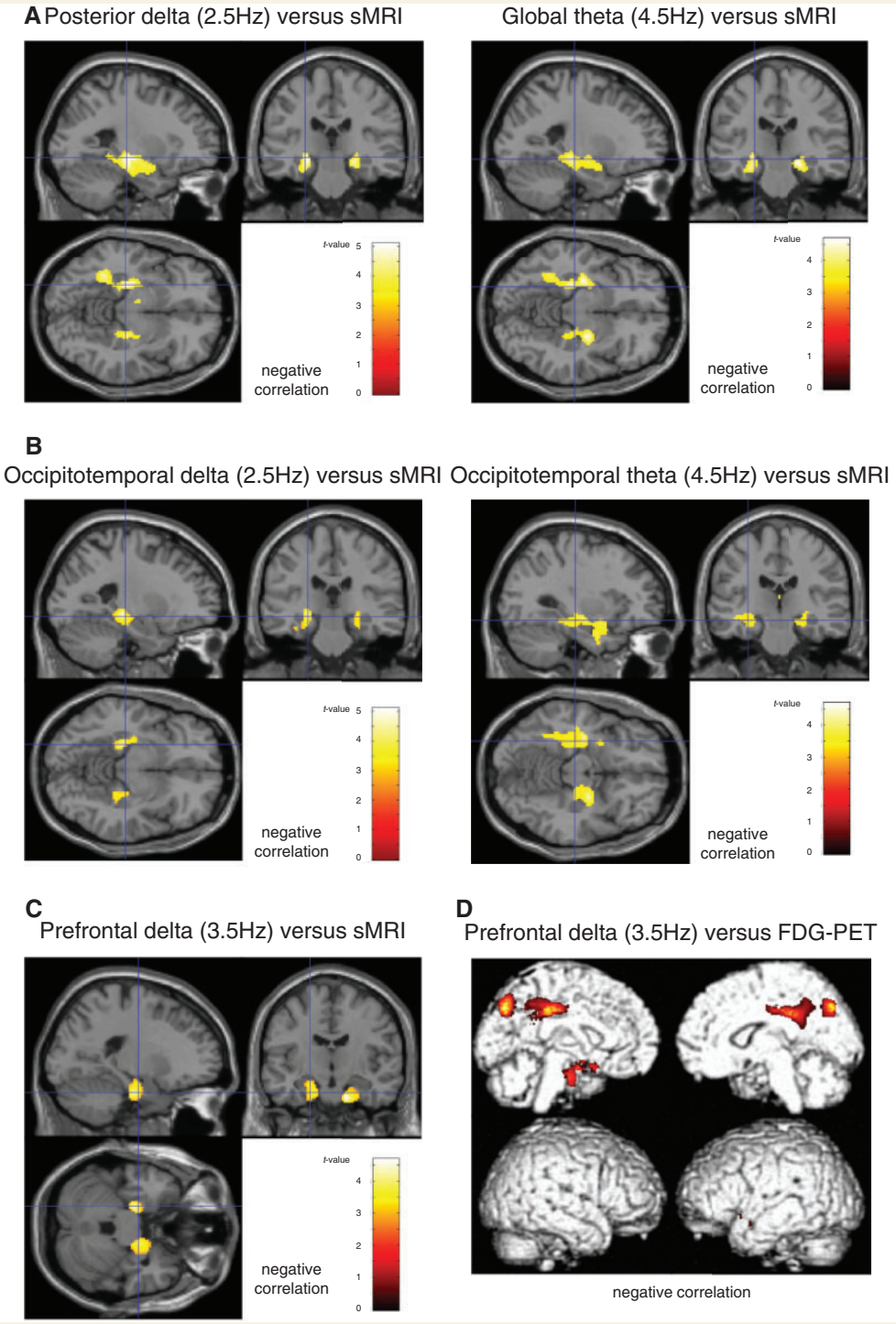

Figure 4 Multiple regression analysis between the power marker values and regional grey matter volume (A–C) or regional glucose metabolism (D), adjusting for the effects of age. (**A**) Results of multiple regression analysis using whole-brain voxel-based morphometry (VBM) for power markers that represent the main effects of clinical category in all subjects ($n = 66$). *Left*: Delta power at 2.5 Hz in the posterior part of the brain. *Right*: Theta power at 4.5 Hz in the global brain. Regions in which the grey matter volumes showed significant negative correlations (FWE-corrected $P < 0.05$ at a height threshold of $P = 0.001$, adjusted for the effects of age) were visualized. (**B**) Results of VBM for the power markers that represent the effects of clinical category within the amyloid-β-negative groups (CNn and MCIn, $n = 28$). *Left:* Delta power at 2.5 Hz in the occipitotemporal areas (FWE-corrected $P < 0.05$ at a height threshold of $P = 0.001$). *Right*: Theta power at 4.5 Hz in the occipitotemporal areas (FWE-corrected $P < 0.05$ at a height threshold of $P = 0.005$). (**C**) Results of VBM analyses for power markers that represent the effects of clinical category within the amyloid-β-positive groups (CNp and MCIp, $n = 38$) as 3.5-Hz delta power in the medial prefrontal areas (FWE-corrected $P < 0.05$ at a height threshold of $P = 0.005$). (**D**) Results of multiple regression analysis of FDG-PET images in the amyloid-β-positive groups (CNp and MCIp, $n = 38$) for the same power marker as **C**. Statistically significant clusters in which regional glucose metabolism showed significant negative correlations with the power marker values are visualized (FWE-corrected $P < 0.05$ at a height threshold of $P = 0.001$). sMRI = structural MRI.

2011; Lim *et al.*, 2014*a*; Jones *et al.*, 2015). Although the methodological approach of our study is different from these earlier studies (power spectrum versus functional connectivity), common pathophysiological mechanisms may exist that are related to the frontal functional upregulation. We consider two possible explanations for this. The first hypothesis is a compensatory mechanism, which was also proposed in previous studies (Qi *et al.*, 2010; Mormino *et al.*, 2011; Lim *et al.*, 2014*a*; Jones *et al.*, 2015). Our results showed a stronger topographical association with a dose-dependent effect between the prefrontal alpha augmentation and prefrontal amyloid-β burden in the CN groups than in the MCI groups and may support this compensatory hypothesis. This is because a sufficient level of compensation is needed to maintain normal cognitive function in the preclinical stages of Alzheimer's disease, whereas this compensation probably becomes insufficient in the prodromal Alzheimer's disease stage. The second hypothesis is abnormal hyperexcitability related to amyloid-β deposition. Palop and Mucke (2010) reported a strong influence of amyloid-β in the destabilization of cortical network activity. Busche *et al.* (2008) demonstrated that clusters of neurons near amyloid plaques become hyperactive, and suggested that this hyperactivity is caused by a relative decrease in synaptic inhibition. This finding was reinforced by a histological study by García-Marín and coworkers (2009), who showed diminished GABAergic terminals in the vicinity of amyloid plaques. These previous studies may support the hyperexcitability hypothesis.

In our study, significant relationships were found between the prefrontal alpha power and local amyloid-β deposition only in group-wise comparisons, but not in the two-way analysis, although the latter revealed a significant main effect of amyloid-β deposition. We consider that this could be due to the differences between the CN and MCI groups in the peak alpha power frequency that showed an amyloid effect. In the group-wise analyses, the peak alpha power frequencies were 9 Hz and 10.5 Hz, respectively, whereas the peak frequency showing the main effect was 9.5 Hz in the two-way analysis. This may indicate that the correlations between the prefrontal alpha power and local amyloid-β deposition were significant only around the peak frequency of alpha power in each clinical category.

The power markers that represented effects of amyloid-β deposition did not show a significant correlation with any of the cognitive measures. This was in line with a previous report (Jack *et al.*, 2009) suggesting that clinical symptoms are not coupled with amyloid-β deposition. In general, downstream topographical markers such as regional glucose hypometabolism measured by FDG-PET and medial temporal atrophy assessed by structural MRI are not considered specific to amyloid-β pathology, especially in the preclinical stage of Alzheimer's disease (Dubois *et al.*, 2016). Therefore, potential amyloid-β-related biomarker information may be one of the unique features of the MEG markers.

Effects of clinical status on regional power spectra

In the two-way analyses, the main effects of the clinical status were represented as widespread power augmentation within the low-frequency bands (delta and theta) in the MCI groups compared with the CN groups. The power values were significantly correlated with cognitive decline and hippocampal atrophy. In addition, the MCI groups also showed reduced alpha power in the prefrontal areas. These findings were similar to typical spectral patterns observed in previous reports that compared MCI and CN groups (Babiloni *et al.*, 2006; Fernández *et al.*, 2006*b*, 2013; Rossini *et al.*, 2007; Stam, 2010; Lizio *et al.*, 2011; López *et al.*, 2016). However, when subjects were further segregated based on amyloid-β positivity, group-wise comparisons revealed additional important findings that are crucial for understanding the relevance of regional spectral patterns to their pathophysiological backgrounds.

The group-wise comparison within the amyloid-β-negative groups (MCIn versus CNn) demonstrated similar findings with the two-way comparison. The MCIn group showed increased delta and theta power in rather widespread areas and decreased alpha power in the prefrontal region compared with the CNn group. This is important because such power spectral features were previously considered to be changes related to the progression of Alzheimer's disease (Fernández *et al.*, 2006*a*; Rossini *et al.*, 2007). However, the results indicated that these changes are not specific to Alzheimer's disease and can be observed without Alzheimer's disease pathology (i.e. amyloid-β deposition). A further important finding was that the power marker values, especially the delta and theta power increase in the posterior brain regions, were significantly correlated with cortical atrophy, specifically in the hippocampus. Recently, the suspected non-Alzheimer disease pathophysiology (SNAP) concept was developed, which suggests the presence of a significant amyloid-β-negative population with biomarker evidence of neurodegeneration (Jack *et al.*, 2016). The prevalence of SNAP is considered to be around 25% in individuals with MCI and CN (Vos *et al.*, 2015; Burnham *et al.*, 2016; Mormino *et al.*, 2016). In fact, 4/25 and 5/11 subjects in the CNn and MCIn groups, respectively (in total 9/36 = 25%), had VSRAD scores >1.0 in our sample, which matches the reported prevalence. Although SNAP represents a heterogeneous status with different pathological aetiologies (Jack *et al.*, 2016; Mormino *et al.*, 2016), delta and theta power augmentation in posterior brain regions may be associated with disease progression within a particular SNAP status.

The results of the group-wise comparison within the amyloid-β-positive groups (MCIp versus CNp) provided even more important information, because they highlighted the regional spectral pattern related to disease progression

within the Alzheimer's disease continuum. They were expressed as delta power augmentation in the medial prefrontal and occipital regions in the MCIp group compared to the CNp group. Both markers were significantly correlated with cognitive scores. In particular, the medial prefrontal delta power appeared to be an important MEG marker, because it was significantly correlated with other imaging markers that serve as surrogates for disease progression, including cortical atrophy in the entorhinal cortex and Alzheimer's disease-like regional glucose hypometabolism. This finding is in line with our previous report suggesting that delta activity in the anterior and occipital brain regions is associated with disease progression (Fernández *et al.*, 2013; López *et al.*, 2016). These results suggest that medial prefrontal power augmentation is coupled with neurodegeneration, and is expected to be useful for monitoring disease progression in the preclinical and prodromal stages of Alzheimer's disease.

Potential clinical utility of the MEG power markers

To estimate the potential clinical utility of the MEG power markers that showed significant group effects of amyloid-β deposition, we evaluated performances to distinguish between amyloid-β-positive and amyloid-β-negative individuals using ROC analyses. Results demonstrated that within the CN groups, the prefrontal alpha power at 10.5 Hz could predict amyloid-β positivity with an area under the curve (AUC) of 0.788 and accuracy of 0.763 (Supplementary Fig. 3A and Supplementary Table 2). Within the MCI groups, the prefrontal alpha power at 9 Hz showed performance with an AUC of 0.866 and

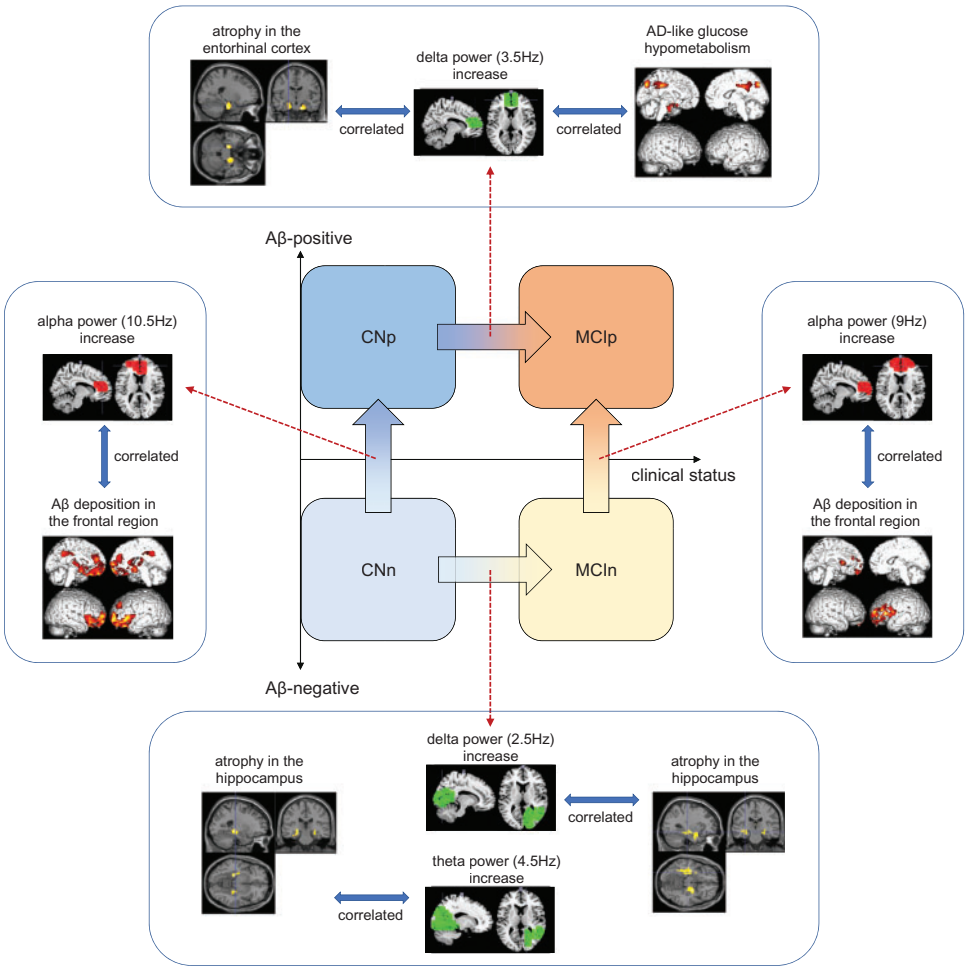

Figure 5 A schematic summarizing the main findings. The left and right red arrows and their connected boxes demonstrate the characteristics of the MEG power markers that represented the effects of amyloid-β deposition within the CN groups and within the MCI groups, respectively. The upper and lower red arrows and their connected boxes demonstrate the characteristics of the MEG power markers that represented the effects of clinical category within the amyloid-β-positive groups and within the amyloid-β-negative groups, respectively. The arrows with the gradation colours indicate the directions where the relative power increases (not indicating clinical transition).

accuracy of 0.786 (Supplementary Fig. 3B and Supplementary Table 3).

To identify individuals who showed medial temporal atrophy, we also used ROC analyses to estimate the performances of power markers that showed significant correlations with the grey matter volume in the medial temporal areas. For the analyses, the degree of medial temporal atrophy was dichotomized using the VSRAD scores with a cut-off value of 1.0 (Supplementary Fig. 1). Values lower than the cut-off point suggested that the medial temporal regions were not atrophic. Among the power markers representing the main effects of clinical status, the global theta power augmentation at 4.5 Hz demonstrated the highest performance with an AUC of 0.833 and accuracy of 0.773 (Supplementary Fig. 4A and Supplementary Table 4). For the power markers representing group effects within the amyloid-β-negative groups, the occipitotemporal theta power showed the highest performance with an AUC of 0.831 and accuracy of 0.806 (Supplementary Fig. 4B and Supplementary Table 4). The power marker representing the within-amyloid-β-positive group effects as delta (3.5 Hz) power augmentation in the prefrontal areas showed an AUC of 0.880 and accuracy of 0.867 (Supplementary Fig. 4C and Supplementary Table 4).

However, because these analyses, especially for the amyloid-β markers, could be circular, these values should be only interpreted as references, and validation in an independent dataset is required.

Limitations of this study

The present study is limited because of the relatively small sample size and the lack of follow-up information. Validation studies should be carried out with larger sample sizes, preferably coupled with follow-up information. Tau marker information was also not available, which also limits the scope of this study. Combining our methods with direct tau markers, such as CSF or tau PET imaging markers, may deepen our understanding of the association between MEG signatures and their pathophysiological implications.

Conclusion

This investigation demonstrated that the regional spectral patterns of resting state MEG activity in MCI and CN subjects conveyed complex information derived from different pathophysiological backgrounds. By incorporating the biomarker information for amyloid-β deposition and neurodegeneration, complex MEG signatures were successfully revealed as summarized in Fig. 5. These findings suggest that MEG potentially offers the following biomarker information: (i) the power augmentation in the alpha band in the medial prefrontal regions is a surrogate marker for amyloid-β pathology both in the CN and MCI groups, and the topographical association with the local amyloid-β burden is stronger in the CN group than the MCI group; (ii) the delta power increase in the medial frontal region is a surrogate marker for disease progression within the Alzheimer's disease continuum, and is associated with downstream changes, including cortical atrophy in the entorhinal cortex, and Alzheimer's disease-like regional glucose hypometabolism; and (iii) delta and theta power augmentation in posterior brain regions is a surrogate marker for hippocampal atrophy and general cognitive decline, and the power changes can be observed without amyloid-β pathology, indicating that the signature is not specific to Alzheimer's disease. These MEG signatures are also expected to deepen the understanding of the pathophysiological processes of disease progression in predementia stages of Alzheimer's disease.

Acknowledgements

We sincerely thank all the clinical doctors, researchers, and staff at the National Center for Geriatrics and Gerontology (NCGG) who supported the MULNIAD project. The MULNIAD project is registered as UMIN ID: 000006419 and 000016144.

Funding

This study was supported by the Research Funding for Longevity Sciences (23-26, 25-24, and 26-30) from the NCGG and the Japan Society for the Promotion of Science (JSPS) (KAKENHI Grant Number 24590908). The funding sources had no role in the study design, data collection, data analyses, or data interpretation.

Supplementary material

Supplementary material is available at *Brain* online.

References

Albert MS, DeKosky ST, Dickson D, Dubois B, Feldman HH, Fox NC, et al. The diagnosis of mild cognitive impairment due to Alzheimer's disease: recommendations from the National Institute on Aging-Alzheimer's Association workgroups on diagnostic guidelines for Alzheimer's disease. Alzheimers Dement 2011; 7: 270–9.

Anchisi D, Borroni B, Franceschi M, Kerrouche N, Kalbe E, Beuthien-Beumann B, et al. Heterogeneity of brain glucose metabolism in mild cognitive impairment and clinical progression to Alzheimer disease. Arch Neurol 2005; 62: 1728–33.

Babiloni C, Binetti G, Cassetta E, Dal Forno G, Del Percio C, Ferreri F, et al. Sources of cortical rhythms change as a function of cognitive impairment in pathological aging: a multicenter study. Clin Neurophysiol 2006; 117: 252–68.

Bateman RJ, Xiong C, Benzinger TLS, Fagan AM, Goate A, Fox NC, et al. Clinical and biomarker changes in dominantly inherited Alzheimer's disease. N Engl J Med 2012; 367: 795–804.

Blennow K, Hampel H, Weiner M, Zetterberg H. Cerebrospinal fluid and plasma biomarkers in Alzheimer disease. Nat Rev Neurol 2010; 6: 131–44.

Buckner RL, Andrews-Hanna JR, Schacter DL. The brain's default network: anatomy, function, and relevance to disease. Ann N Y Acad Sci 2008; 1124: 1–38.

Burnham SC, Bourgeat P, Doré V, Savage G, Brown B, Laws S, et al. Clinical and cognitive trajectories in cognitively healthy elderly individuals with Suspected Non-Alzheimer's Disease Pathophysiology (SNAP) or Alzheimer's disease pathology: a longitudinal study. Lancet Neurol 2016; 4422: 1–10.

Busche MA, Eichhoff G, Adelsberger H, Abramowski D, Wiederhold K-H, Haass C, et al. Clusters of hyperactive neurons near amyloid plaques in a mouse model of Alzheimer's disease. Science 2008; 321: 1686–9.

Chételat G, Villemagne VL, Villain N, Jones G, Ellis KA, Ames D, et al. Accelerated cortical atrophy in cognitively normal elderly with high β-amyloid deposition. Neurology 2012; 78: 477–84.

Cuesta P, Barabash A, Aurtenetxe S, Garcés P, López ME, Bajo R, et al. Source analysis of spontaneous magnetoencephalograpic activity in healthy aging and mild cognitive impairment: influence of apolipoprotein E polymorphism. J Alzheimers Dis 2014; 43: 259–73.

Cummings J, Aisen P, Barton R, Bork J, Doody R, Dwyer J, et al. Re-engineering Alzheimer clinical trials: global Alzheimer's platform network. J Prev Alzheimers Dis 2016; 3: 114–20.

Doré V, Villemagne VL, Bourgeat P, Fripp J, Acosta O, Chetélat G, et al. Cross-sectional and longitudinal analysis of the relationship between Aβ deposition, cortical thickness, and memory in cognitively unimpaired individuals and in Alzheimer disease. JAMA Neurol 2013; 70: 903–11.

de Waal H, Stam CJ, de Haan W, van Straaten ECW, Blankenstein MA, Scheltens P, et al. Alzheimer's disease patients not carrying the apolipoprotein ε4 allele show more severe slowing of oscillatory brain activity. Neurobiol. Aging 2013; 34: 2158–63.

Drzezga A, Lautenschlager N, Siebner H, Riemenschneider M, Willoch F, Minoshima S, et al. Cerebral metabolic changes accompanying conversion of mild cognitive impairment into Alzheimer's disease: a PET follow-up study. Eur J Nucl Med Mol Imaging 2003; 30: 1104–13.

Dubois B, Feldman HH, Jacova C, Cummings JL, DeKosky ST, Barberger-Gateau P, et al. Revising the definition of Alzheimer's disease: a new lexicon. Lancet Neurol 2010; 9: 1118–27.

Dubois B, Feldman HH, Jacova C, Hampel H, Molinuevo JL, Blennow K, et al. Advancing research diagnostic criteria for Alzheimer's disease: the IWG-2 criteria. Lancet Neurol 2014; 13: 614–29.

Dubois B, Hampel H, Feldman HH, Scheltens P, Aisen P, Andrieu S, et al. Preclinical Alzheimer's disease: definition, natural history, and diagnostic criteria. Alzheimers Dement 2016; 12: 292–323.

Engels MM, Hillebrand A, van der Flier WM, Stam CJ, Scheltens P, van Straaten ECW. Slowing of hippocampal activity correlates with cognitive decline in early onset Alzheimer's disease. An MEG study with virtual electrodes. Front Hum Neurosci 2016; 10: 1–13.

Fernández A, Arrazola J, Maestú F, Amo C, Gil-Gregorio P, Wienbruch C, et al. Correlations of hippocampal atrophy and focal low-frequency magnetic activity in Alzheimer disease: volumetric MR imaging-magnetoencephalographic study. Am J Neuroradiol 2003; 24: 481–7.

Fernández A, Hornero R, Mayo A, Poza J, Gil-Gregorio P, Ortiz T. MEG spectral profile in Alzheimer's disease and mild cognitive impairment. Clin Neurophysiol 2006a; 117: 306–14.

Fernández A, Turrero A, Zuluaga P, Gil-Gregorio P, Del Pozo F, Maestu F, et al. MEG delta mapping along the healthy aging-alzheimer's disease continuum: diagnostic implications. J Alzheimers Dis 2013; 35: 495–507.

Fernández A, Turrero A, Zuluaga P, Gil P, Maestú F, Campo P, et al. Magnetoencephalographic parietal delta dipole density in mild cognitive impairment: preliminary results of a method to estimate the risk of developing Alzheimer disease. Arch Neurol 2006b; 63: 427–30.

García-Marín V, Blazquez-Llorca L, Rodriguez J-R, Boluda S, Muntane G, Ferrer I, et al. Diminished perisomatic GABAergic terminals on cortical neurons adjacent to amyloid plaques. Front Neuroanat 2009; 3: 28.

Gouw AA, Alsema AM, Tijms BM, Borta A, Scheltens P, Stam CJ, et al. EEG spectral analysis as a putative early prognostic biomarker in nondemented, amyloid positive subjects. Neurobiol Aging 2017; 57: 133–42.

Harada R, Okamura N, Furumoto S, Furukawa K, Ishiki A, Tomita N, et al. 18F-THK5351: a novel PET radiotracer for imaging neurofibrillary pathology in Alzheimer disease. J Nucl Med 2016; 57: 208–14.

Jack CR, Knopman DS, Chételat G, Dickson D, Fagan AM, Frisoni GB, et al. Suspected non-Alzheimer disease pathophysiology—concept and controversy. Nat Rev Neurol 2016; 12: 117–24.

Jack CR, Knopman DS, Jagust WJ, Petersen RC, Weiner MW, Aisen PS, et al. Tracking pathophysiological processes in Alzheimer's disease: an updated hypothetical model of dynamic biomarkers. Lancet Neurol 2013; 12: 207–16.

Jack CR, Lowe VJ, Weigand SD, Wiste HJ, Senjem ML, Knopman DS, et al. Serial PIB and MRI in normal, mild cognitive impairment and Alzheimer's disease: implications for sequence of pathological events in Alzheimer's disease. Brain 2009; 132: 1355–65.

Jelic V, Blomberg M, Dierks T, Basun H, Shigeta M, Julin P, et al. EEG slowing and cerebrospinal fluid tau levels in patients with cognitive decline. Neuroreport 1998; 9: 157–60.

Jelic V, Johansson SE, Almkvist O, Shigeta M, Julin P, Nordberg A, et al. Quantitative electroencephalography in mild cognitive impairment: longitudinal changes and possible prediction of Alzheimer's disease. Neurobiol Aging 2000; 21: 533–40.

Jones DT, Knopman DS, Gunter JL, Graff-Radford J, Vemuri P, Boeve BF, et al. Cascading network failure across the Alzheimer's disease spectrum. Brain 2015; 139: 547–62.

Kaneko N, Nakamura A, Washimi Y, Kato T, Sakurai T, Arahata Y, et al. Novel plasma biomarker surrogating cerebral amyloid deposition. Proc Jpn Acad Ser B Phys Biol Sci 2014; 90: 353–64.

Kramberger MG, Kåreholt I, Andersson T, Winblad B, Eriksdotter M, Jelic V. Association between EEG abnormalities and csf biomarkers in a memory clinic cohort. Dement Geriatr Cogn Disord 2013; 36: 319–28.

Larrieu S, Letenneur L, Orgogozo JM, Fabrigoule C, Amieva H, Le Carret N, et al. Incidence and outcome of mild cognitive impairment in a population-based prospective cohort. Neurology 2002; 59: 1594–9.

Lehtovirta M, Partanen J, Könönen M, Soininen H, Helisalmi S, Mannermaa A, et al. Spectral analysis of EEG in Alzheimer's disease: relation to apolipoprotein E polymorphism. Neurobiol Aging 1996; 17: 523–6.

Lim HK, Nebes R, Snitz B, Cohen A, Mathis C, Price J, et al. Regional amyloid burden and intrinsic connectivity networks in cognitively normal elderly subjects. Brain 2014a; 137: 3327–38.

Lim YY, Maruff P, Pietrzak RH, Ames D, Ellis KA, Harrington K, et al. Effect of amyloid on memory and non-memory decline from preclinical to clinical Alzheimer's disease. Brain 2014b; 137: 221–31.

Lizio R, Vecchio F, Frisoni GB, Ferri R, Rodriguez G, Babiloni C. Electroencephalographic rhythms in Alzheimer's disease. Int J Alzheimers Dis 2011; 2011: 927573.

López ME, Bruna R, Aurtenetxe S, Pineda-Pardo JA, Marcos A, Arrazola J, et al. Alpha-band hypersynchronization in progressive mild cognitive impairment: a magnetoencephalography study. J Neurosci 2014a; 34: 14551–9.

López ME, Cuesta P, Garcés P, Castellanos PN, Aurtenetxe S, Bajo R, et al. MEG spectral analysis in subtypes of mild cognitive impairment. Age 2014b; 36: 9624.

López ME, Turrero A, Cuesta P, López-Sanz D, Bruña R, Marcos A, et al. Searching for primary predictors of conversion from mild

cognitive impairment to Alzheimer's disease: a multivariate follow-up study. J Alzheimers Dis 2016; 52: 133–43.
Maris E, Oostenveld R. Nonparametric statistical testing of EEG- and MEG-data. J Neurosci Methods 2007; 164: 177–90.
Maruyama M, Shimada H, Suhara T, Shinotoh H, Ji B, Maeda J, et al. Imaging of tau pathology in a tauopathy mouse model and in Alzheimer patients compared to normal controls. Neuron 2013; 79: 1094–108.
Matsuda H. Voxel-based morphometry of brain MRI in normal aging and Alzheimer's disease. Aging Dis 2013; 4: 29–37.
Matsuda H, Mizumura S, Nemoto K, Yamashita F, Imabayashi E, Sato N, et al. Automatic voxel-based morphometry of structural MRI by SPM8 plus diffeomorphic anatomic registration through exponentiated lie algebra improves the diagnosis of probable Alzheimer disease. AJNR Am J Neuroradiol 2012; 33: 1109–14.
McKhann GM, Knopman DS, Chertkow H, Hyman BT, Jack CR, Kawas CH, et al. The diagnosis of dementia due to Alzheimer's disease: recommendations from the National Institute on Aging-Alzheimer's Association workgroups on diagnostic guidelines for Alzheimer's disease. Alzheimers Dement 2011; 7: 263–9.
Mintun MA, Larossa GN, Sheline YI, Dence CS, Lee SY, Mach RH, et al. [11C]PIB in a nondemented population: potential antecedent marker of Alzheimer disease. Neurology 2006; 67: 446–52.
Mormino EC, Papp KV, Rentz DM, Schultz AP, LaPoint M, Amariglio R, et al. Heterogeneity in Suspected Non–Alzheimer Disease Pathophysiology among clinically normal older individuals. JAMA Neurol 2016; 73: 1185–91.
Mormino EC, Smiljic A, Hayenga AO, Onami SH, Greicius MD, Rabinovici GD, et al. Relationships between beta-amyloid and functional connectivity in different components of the default mode network in aging. Cereb Cortex 2011; 21: 2399–407.
Morris JC. Early-stage and preclinical Alzheimer disease. Alzheimer Dis Assoc Disord 2005; 19: 163–5.
Mosconi L. Brain glucose metabolism in the early and specific diagnosis of Alzheimer's disease. FDG-PET studies in MCI and AD. Eur J Nucl Med Mol Imaging 2005; 32: 486–510.
Nakamura A, Cuesta P, Kato T, Arahata Y, Iwata K, Yamagishi M, et al. Early functional network alterations in asymptomatic elders at risk for Alzheimer's disease. Sci Rep 2017; 7: 6517.
Oostenveld R, Fries P, Maris E, Schoffelen J-M. FieldTrip: open source software for advanced analysis of MEG, EEG, and invasive electrophysiological data. Comput Intell Neurosci 2011; 2011: 156869.
Palop JJ, Mucke L. Amyloid-beta-induced neuronal dysfunction in Alzheimer's disease: from synapses toward neural networks. Nat Neurosci 2010; 13: 812–18.
Prichep LS. Quantitative EEG and electromagnetic brain imaging in aging and in the evolution of dementia. Ann N Y Acad Sci 2007; 1097: 156–67.
Qi Z, Wu X, Wang Z, Zhang N, Dong H, Yao L, et al. Impairment and compensation coexist in amnestic MCI default mode network. Neuroimage 2010; 50: 48–55.
Rabinovici GD, Rosen HJ, Alkalay A, Kornak J, Furst AJ, Agarwal N, et al. Amyloid vs FDG-PET in the differential diagnosis of AD and FTLD. Neurology 2011; 77: 2034–42.
Riekkinen P, Sirviö J. Relationship between the cortical choline acetyltransferase content and EEG delta-power. Neurosci Res 1990; 8: 12–20.
Risacher SL, Saykin AJ, West JD, Shen L, Firpi HA, McDonald BC, et al. Baseline MRI predictors of conversion from MCI to probable AD in the ADNI cohort. Curr Alzheimer Res 2009; 6: 347–61.
Ritchie CW, Molinuevo JL, Truyen L, Satlin A, Van der Geyten S, Lovestone S. Development of interventions for the secondary prevention of Alzheimer's dementia: the European Prevention of Alzheimer's Dementia (EPAD) project. Lancet Psychiatry 2016; 3: 179–86.
Rodriguez G, Nobili F, Rocca G, De Carli F, Gianelli MV, Rosadini G. Quantitative electroencephalography and regional cerebral blood flow: discriminant analysis between Alzheimer's patients and healthy controls. Dement Geriatr Cogn Disord 1998; 9: 274–83.
Rossini PM, Rossi S, Babiloni C, Polich J. Clinical neurophysiology of aging brain: from normal aging to neurodegeneration. Prog Neurobiol 2007; 83: 375–400.
Sevigny J, Chiao P, Bussière T, Weinreb PH, Williams L, Maier M, et al. The antibody aducanumab reduces Aβ plaques in Alzheimer's disease. Nature 2016; 537: 50–6.
Small GW, Ercoli LM, Silverman DH, Huang SC, Komo S, Bookheimer SY, et al. Cerebral metabolic and cognitive decline in persons at genetic risk for Alzheimer's disease. Proc Natl Acad Sci USA 2000; 97: 6037–42.
Snowdon DA. Aging and Alzheimer's disease: lessons from the Nun Study. Gerontologist 1997; 37: 150–6.
Sperling RA, Aisen PS, Beckett LA, Bennett DA, Craft S, Fagan AM, et al. Toward defining the preclinical stages of Alzheimer's disease: recommendations from the National Institute on Aging-Alzheimer's Association workgroups on diagnostic guidelines for Alzheimer's disease. Alzheimers Dement 2011; 7: 280–92.
Sperling RA, Rentz DM, Johnson KA, Karlawish J, Donohue M, Salmon DP, et al. The A4 study: stopping AD before symptoms begin? Sci Transl Med 2014; 6: 228fs13.
Stam CJ. Use of magnetoencephalography (MEG) to study functional brain networks in neurodegenerative disorders. J Neurol Sci 2010; 289: 128–34.
Stomrud E, Hansson O, Minthon L, Blennow K, Rosén I, Londos E. Slowing of EEG correlates with CSF biomarkers and reduced cognitive speed in elderly with normal cognition over 4 years. Neurobiol Aging 2010; 31: 215–23.
Storandt M, Mintun MA, Head D, Morris JC. Cognitive decline and brain volume loss as signatures of cerebral amyloid-beta peptide deposition identified with Pittsburgh compound B: cognitive decline associated with Abeta deposition. Arch Neurol 2009; 66: 1476–81.
Tzourio-Mazoyer N, Landeau B, Papathanassiou D, Crivello F, Etard O, Delcroix N, et al. Automated anatomical labeling of activations in SPM using a macroscopic anatomical parcellation of the MNI MRI single-subject brain. Neuroimage 2002; 15: 273–89.
Van Veen BD, van Drongelen W, Yuchtman M, Suzuki A. Localization of brain electrical activity via linearly constrained minimum variance spatial filtering. IEEE Trans Biomed Eng 1997; 44: 867–80.
Villemagne VL, Burnham S, Bourgeat P, Brown B, Ellis KA, Salvado O, et al. Amyloid β deposition, neurodegeneration, and cognitive decline in sporadic Alzheimer's disease: a prospective cohort study. Lancet Neurol 2013; 12: 357–67.
Vos SJ, Verhey F, Frölich L, Kornhuber J, Wiltfang J, Maier W, et al. Prevalence and prognosis of Alzheimer's disease at the mild cognitive impairment stage. Brain 2015; 138: 1327–38.
Wolz R, Schwarz AJ, Gray KR, Yu P, Hill DLG; Alzheimer's Disease Neuroimaging Initiative F the ADN. Enrichment of clinical trials in MCI due to AD using markers of amyloid and neurodegeneration. Neurology 2016; 87: 1235–41.